

Three-dimensional numerical simulation of fluid dynamics around vibrating beams

Artem Nuriev

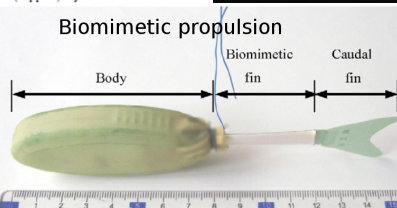
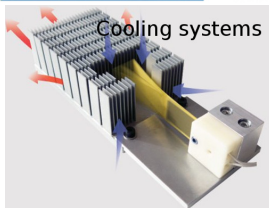
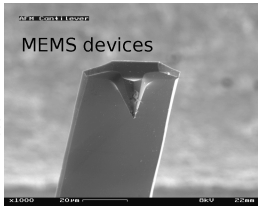
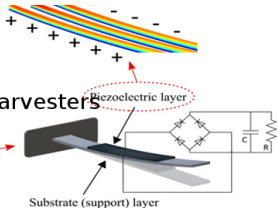
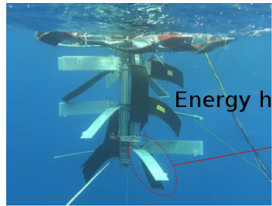


**Kazan Federal
UNIVERSITY**

10.12.20

Motivation for research

Some special applications:



The global goal is to understand the mechanisms of interaction of a beam with a fluid.

Outline

1. 3D simulations

A numerical study of three-dimensional structure of flows caused by elastic flexural vibrations of cantilever beams.

2. Quasi-2-D model

A detailed study of quasi-two-dimensional flows in cross-sections and evaluation of the associated hydrodynamic forces.

3. Experimental measurements

Evaluation of aerodynamic forces acting on oscillating cantilever beams based on the study of the damped flexural vibration of aluminium test samples.

3D simulations. Mathematical formulation

Consider the flow around a cantilever beam with length l , width b and thickness h performing forced bending vibrations. Normalizing the spatial coordinates, time, and velocity we write the governing system of equations of the fluid motion in the form:

$$\frac{\partial U}{\partial t} + U \cdot \nabla U = -\nabla p + \frac{1}{KC\beta} \nabla^2 U, \nabla \cdot U = 0, \quad (1)$$

$$KC = 2\pi \frac{U_0}{b\omega} = 2\pi \frac{A}{b}, \beta = \frac{b^2\omega}{2\pi\nu}.$$

To describe the motion of a beam in a fluid, we use the classical Euler-Bernoulli theory, according to which the position of any point of the beam at an arbitrary time in dimensionless variables is determined by the following formula:

$$w(\xi, t) = \frac{KC}{2\pi} W(\xi) \cos\left(\frac{2\pi}{KC} t\right), \quad \xi = z/l, \quad 0 \leq \xi \leq 1, \quad (2)$$

$$W(\xi) = \frac{1}{2} \left(\cos(k\xi) - \cosh(k\xi) + \frac{\sin k - \sinh k}{\cos k + \cosh k} (\sin(k\xi) - \sinh(k\xi)) \right).$$

3D simulations. Computational method

For discretization of the governing equations we used the finite volume method. The realization of the computation scheme was done on the basis of the **OpenFOAM** package.

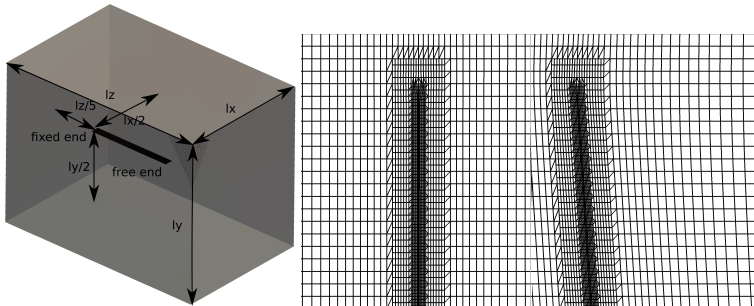


Figure : Computational domain (left) and deformation of the mesh near the lateral edge (right)

3D simulations. Flows around short and long beams

Flows around beams with different relative length $L = l/b$ develop in different ways. Near short beams, ($L = 3, 5$), the essentially three-dimensional flows develop.

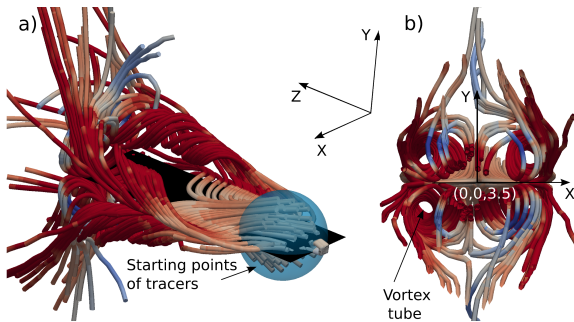


Figure : Visualization of secondary streaming near a **short beam** of length $L = 3$ for $\beta = 430$, $KC = 2$. Pictures (a), (b) are taken from different viewing angles. The lines denote the trajectories of particle tracers released from area near the fixed end.

3D simulations. Flows around short and long beams

The flows forming around **long beam** of ($L = 10, 20$) have a quasi-two-dimensional zone, that covers up to 3/4 of the beam, where transverse flows in cross-sections become dominant.

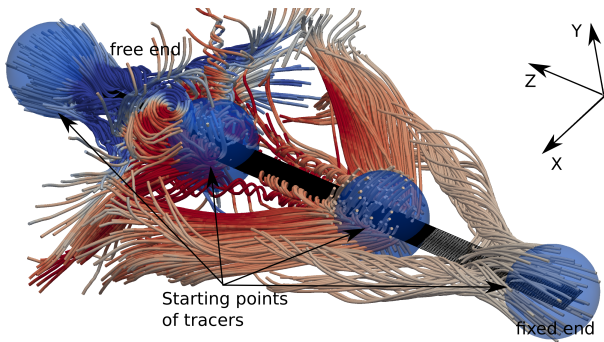


Figure : Visualization of the secondary streaming near a **long beam** of length $L = 20$ for $\beta = 430$, $KC = 2$. The lines denote the trajectories of particle tracers released near the beam.

3D simulations. Flow dynamics around long beams.

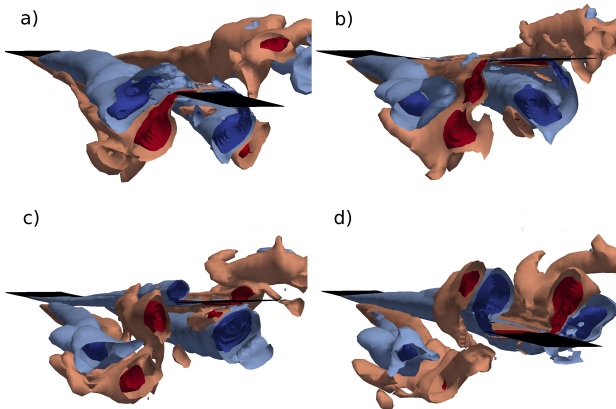


Figure : 3D visualization of the flow. Isosurfaces of the z-component of the vorticity $\Omega_z = \pm[10, 7.77, 5.55, 3.33, 1.3]$ constructed in the region $0 < z < 17$ for $\beta = 200$, $KC = 6$ at time moments $t/T - T_0 = 0(a), 1/6(b), 1/3(c), 1/2(d)$

3D simulations. Flow structure in cross-sections

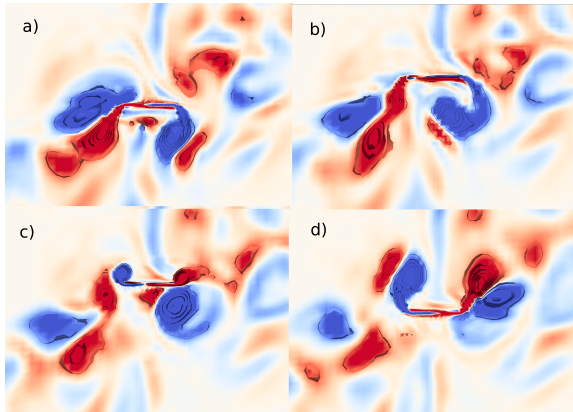


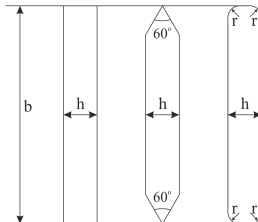
Figure : The cyclic diagonal regime. Isolines of z-component of the vorticity $\Omega_z = \pm[10, 7.77, 5.55, 3.33, 1.3]$ in the cross-section $z = 15.13$ ($KC_{loc} = 4$) for $\beta = 200, KC = 6$ at time moments $t/T - T_0 = 0(a), 1/6(b), 1/3(c), 1/2(d)$

Quasi-2-D model. Analysis of 2D flows past oscillating beam

Quasi-two-dimensional hypothesis:

The motion of a fluid near each beam cross-section at low oscillation modes has a two-dimensional structure that is equivalent to a flow near a harmonically oscillating thin rigid plate.

To check this hypothesis we numerically simulate the flows which formed around beam cross-sections and compare the results with the data of 3D calculations.



Quasi-2-D model. Mathematical formulation of the problem

We will solve the problem in a moving Cartesian coordinate system rigidly connected with the plate. Normalizing the spatial coordinates, time, and velocity, we write the governing system of equations of the fluid motion in the form:

$$\frac{\partial U}{\partial t} + U \cdot \nabla U = -\nabla p + \frac{1}{KC\beta} \nabla^2 U, \nabla \cdot U = 0, \quad (4)$$

$$KC = 2\pi \frac{U_0}{b\omega} = 2\pi \frac{A}{b}, \beta = \frac{b^2\omega}{2\pi\nu}.$$

On the boundary of the plate in the new coordinate system no-slip conditions are specified:

$$u_S = v_S = 0.$$

At infinity the change of the velocity is given by the harmonic law

$$u_\infty = \cos\left(\frac{2\pi}{KC}t\right), v_\infty = 0.$$

Quasi-2-D model. Structure of flows formed by oscillations

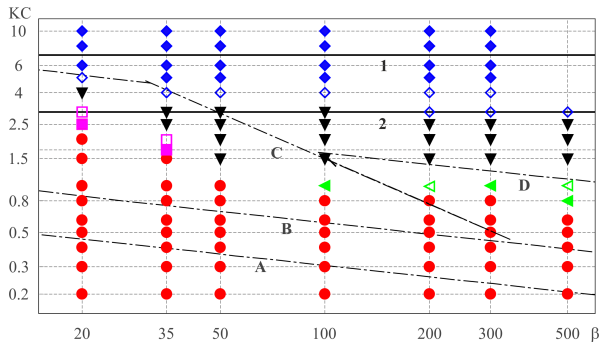


Figure : The flow regimes map. The basic symmetric regime \bullet , the symmetric regime with the attached vortices \blacksquare , the symmetric flow with vertical vortex shedding \blacktriangleleft , regime with a C-shaped structure of the flow \triangleleft , regime with a V-shaped structure of the flow \square , one-sided diagonal \blacktriangledown , stable diagonal (cyclic) regime: \blacklozenge , the unstable diagonal regime \lozenge . The boundaries of the flow regimes according to [Shrestha2018] and [Singh1979] marked with dash-dotted and solid lines, respectively.

Quasi-2-D model. Basic symmetric flow regime

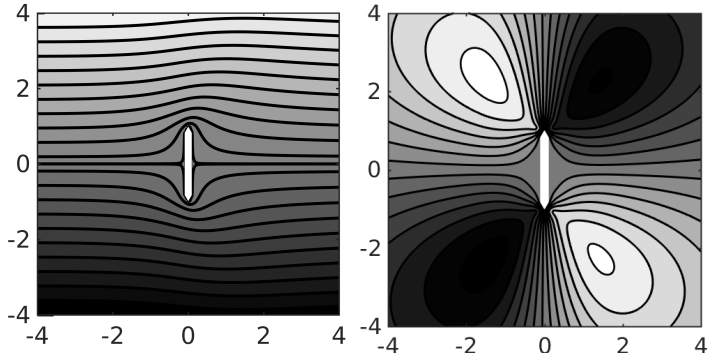


Figure : $\beta = 300$, $KC = 0.2$. a) Instantaneous streamlines at $t/T - T_0 = 0$ ($T_0 = 30$). b) Streamlines of the secondary flow.

Quasi-2-D model. Symmetric flow with attached vortices

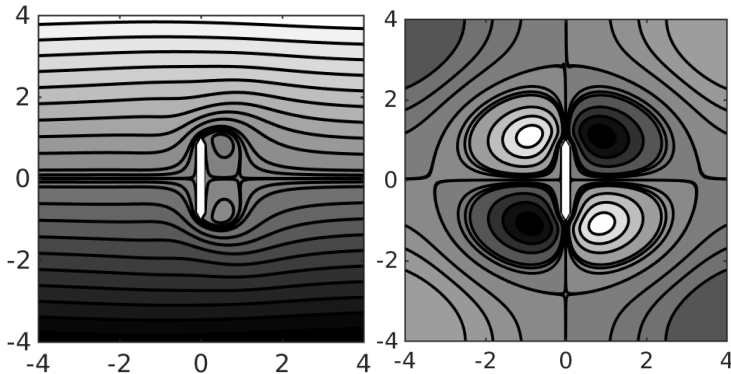


Figure : Symmetric flow with attached vortices at $\beta = 25$, $KC = 2.5$. a) Instantaneous streamlines at $t/T - T_0 = 0$ ($T_0 = 30$). b) Streamlines of the secondary flow.

Quasi-2-D model. Symmetric flow with vertical vortex shedding

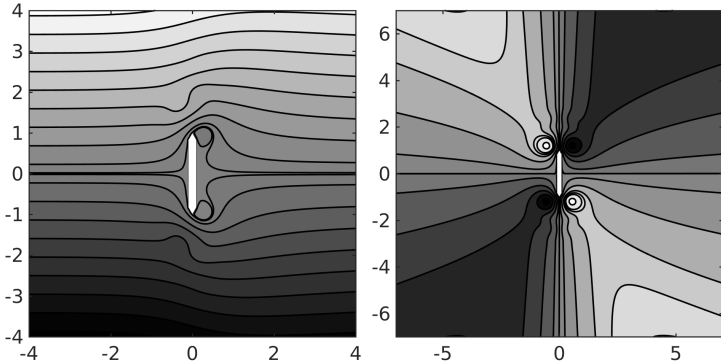


Figure : Symmetric flow with vertical vortex shedding visualized at $\beta = 300$, $KC = 1$. a) Instantaneous streamlines at $t/T - T_0 = 0$ ($T_0 = 30$). b) Streamlines of the secondary flow.

Quasi-2-D model. C-type mechanism of symmetric regimes stability loss

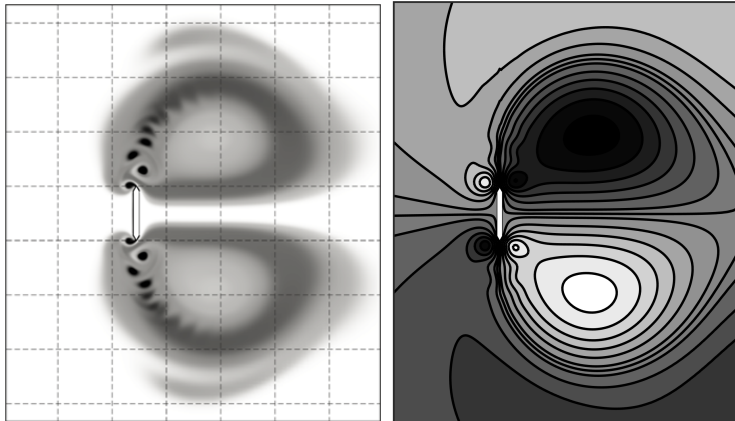


Figure : C-shaped flow regime at $\beta = 500$, $KC = 1$. a) Instantaneous structure of flow obtained using dye; b) Streamlines of the secondary flow.

Quasi-2-D model. V-type mechanism of symmetric regimes stability loss

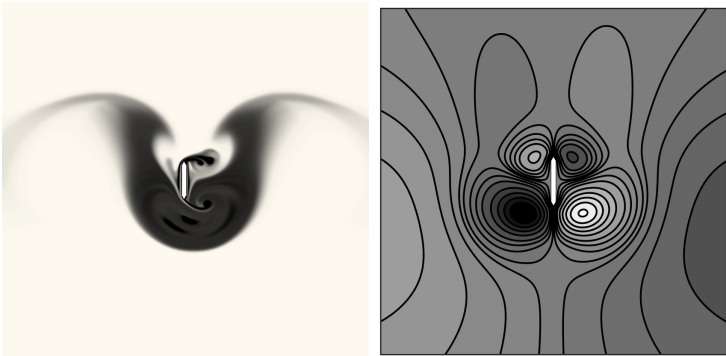
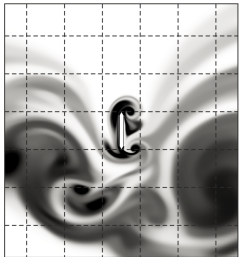
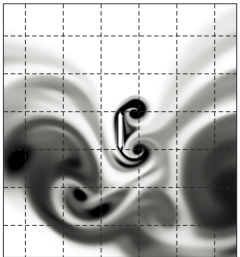


Figure : V-shaped flow regime at $\beta = 20$, $KC = 3.5$. a) Instantaneous structure of flow obtained using dye; b) secondary flow.

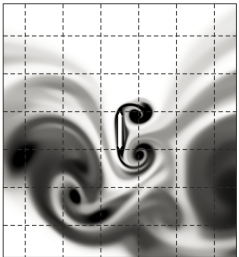
Quasi-2-D model. One-sided diagonal regime at $\beta = 300$,
 $KC = 2.5$



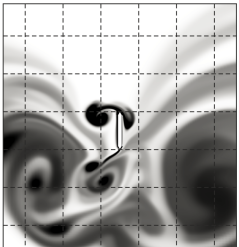
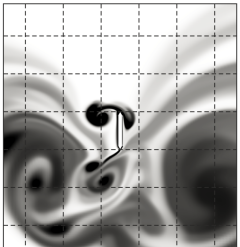
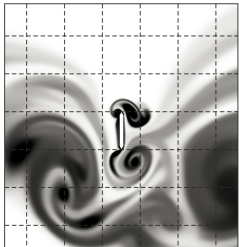
$t/T-T_0=0$



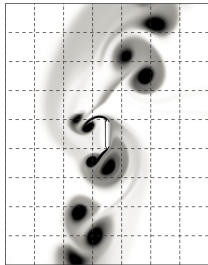
$t/T-T_0=1/8$



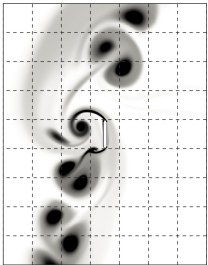
$t/T-T_0=2/8$



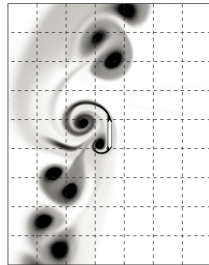
Quasi-2-D model. Two-sided periodic diagonal regime at $\beta = 300$, $KC = 6$



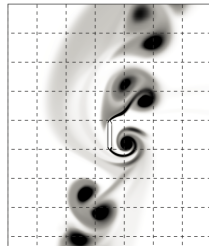
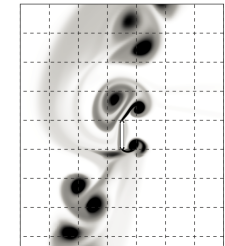
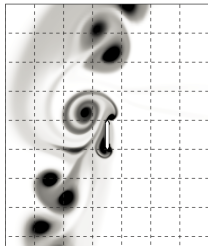
$t/T-T_0=0$



$t/T-T_0=1/8$



$t/T-T_0=2/8$



2D and 3D results comparison. The flow regime map

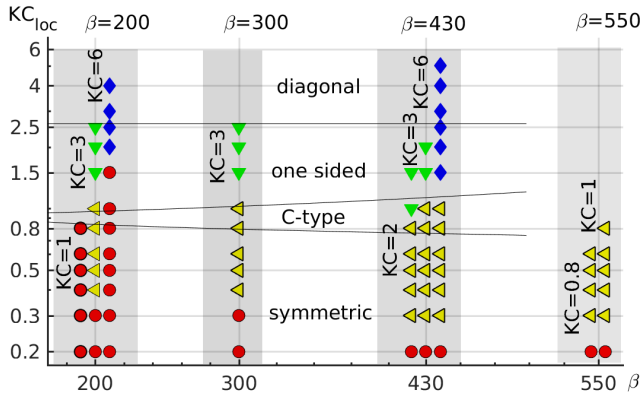
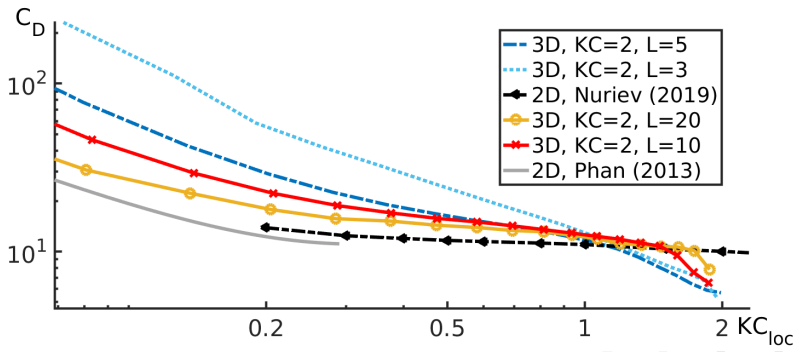


Figure : The flow regime map in the quasi-two-dimensional zone. The symmetric regime: ●, the regime with a C-shaped flow structure: ▷, the one-sided diagonal regime: ▼, the cyclic diagonal regime: ◆. The boundaries of the plane flow regimes are indicated by solid lines.

2D and 3D results comparison. Hydrodynamic forces acting on the beam

We used the Morison approximation to analyze the hydrodynamic forces:

$$F_y(z) = C_M \frac{\pi^2}{KC} W(z/L) \dot{U}_p - C_D W(z/L)^2 |U_p| U_p.$$



3D and 2D comparison. Hydrodynamic forces acting on the beam

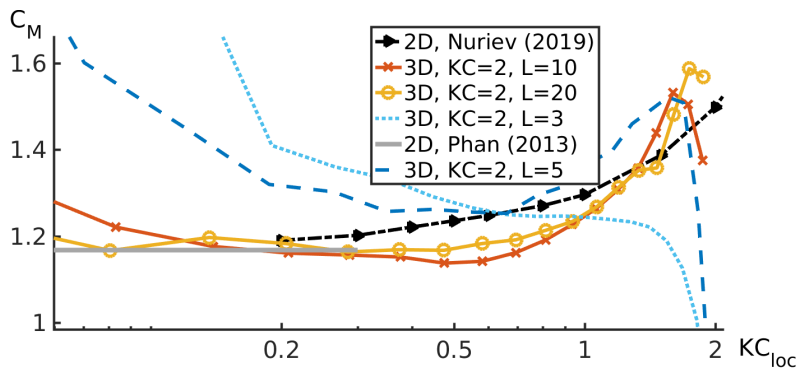


Figure : The distribution of the added mass force coefficient C_M depending on the oscillation amplitude KC_{loc} .

Experimental measurements. Experimental setup

The vibration of the beam was recorded using a 3-axis MEMS gyroscope sensor MPU-6500. The sensor provide the registration of angular velocities in the range $\pm 2000 \text{ deg/s}$ with the sampling rate equals to **8 KHz** and accuracy up to **0.05 deg/sec.**

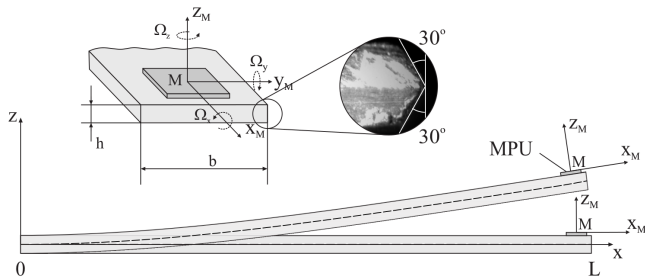


Figure : Installation scheme of MEMS gyroscope on the beam

Experimental measurements. Vibro-record

The MEMS sensor measure 3 angular velocities (Ω_x , Ω_y , Ω_z) with respect to the coordinate system rigidly connected to the beam.

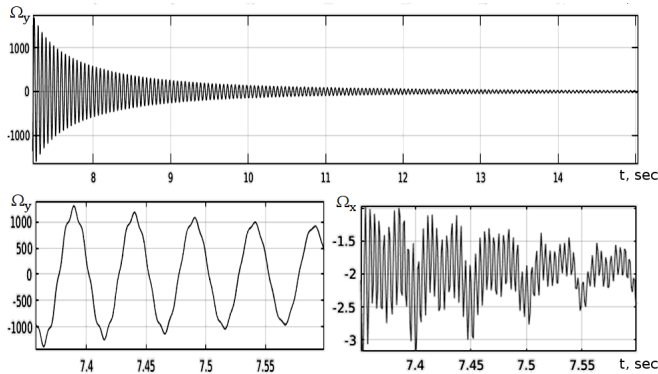


Figure : The angular velocity of the beam vibrations. Data for sample with width $b = 30$ mm and length $L = 180$ mm.

Experimental measurements. Harmonic approximation of the flexural vibrations signal

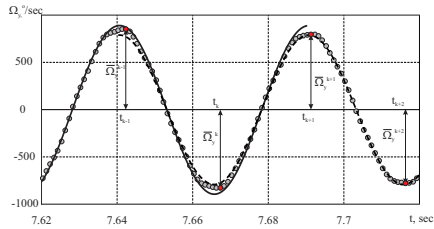


Figure : The angular velocity $\Omega_y(t)$ (round markers) and harmonic approximations $\Omega_y^{Appr}(t)$ of the angular velocity constructed on intervals $[t_{k-1}, t_{k+2}]$ (dotted line) and $[t_{k-3}, t_k]$ (solid line).

To identify the amplitude $A(t)$ and the main frequency ω variations from the signal $\Omega_y(t)$ a harmonic approximation is constructed in the form

$$\varepsilon_k + \Omega_y^k \sin(\omega_k t + t_{0k}).$$

Experimental measurements. Logarithmic decrement ($\delta(\kappa)$) and the relative variation in frequency ($\gamma(\kappa)$)

The obtained approximation is used to calculate the amplitude of flexural vibrations of the free end of the beam

$$A_k = \sin(|\Omega_y^k|/\omega_k) / \frac{dW}{dx}(L), \quad (5)$$

where W is the profile of oscillation.

Then the logarithmic decrement of the beam oscillations $\delta(t)$ and the relative variation in frequency $\gamma(t)$ are calculated as functions of time t

$$\delta(t) = -2\pi\omega_0^{-1} (d(\ln A)/dt), \quad \gamma(t) = (\omega_0 - \omega)/\omega_0. \quad (6)$$

Further, for each experiment in the range of the realized oscillation amplitudes the dependences $\delta(\kappa)$, $\gamma(\kappa)$ are built. Here $\kappa = A/b$.

Experimental measurements. $\delta(\kappa)$ and $\gamma(\kappa)$ as functions of forces

The structure of dependencies $\delta(\kappa), \gamma(\kappa)$ is defined by the forces acting on the beam that consist of external aerodynamic (P) and internal mechanical (H) parts. To analyze this dependencies we conduct two-scale asymptotic expansion. The final result can be represented in the form:

$$\begin{aligned}\delta &= \frac{2\pi}{\rho hbA\omega^2} \{\sin(\omega t) \langle (H + P)W \rangle\} / \langle W^2 \rangle, \\ \gamma &= \frac{1}{\rho hbA\omega^2} \{\cos(\omega t) \langle (H + P)W \rangle\} / \langle W^2 \rangle.\end{aligned}\tag{7}$$

Here and below, angular brackets denote averaging over the spatial coordinate x , and the curly brackets denote averaging over time t . To evaluate the aerodynamic forces, we will accept the hypothesis of a quasi-two-dimensional flow, and the Morison approximation.

Experimental measurements. Determination of the hydrodynamic coefficients

Substituting the approximation of forces into equations for δ and γ , we get the next equations

$$\int_0^1 C_D(\kappa W(\xi)) W^3(\xi) d\xi = \frac{3 \langle W^2 \rangle}{4\kappa} \frac{\rho}{\rho_a} \frac{h}{b} \delta_P(\kappa) . \quad (8)$$
$$\int_0^1 C_M(\kappa W(\xi)) W^2(\xi) d\xi = \frac{8}{\pi} \frac{\rho}{\rho_a} \frac{h}{b} \langle W^2 \rangle \gamma(\kappa)$$

Solving the integral equations, we obtain the following formulas for determination of the hydrodynamic coefficients:

$$C_D(\kappa, \beta) = \frac{9}{32} \frac{\rho}{\rho_a} \frac{h}{b} \kappa^{-8/3} \frac{d}{d\kappa} \left(\kappa^{8/3} (\delta_P(\kappa)) \right) , \quad (9)$$
$$C_M(\kappa, \beta) = \frac{3}{\pi} \frac{\rho}{\rho_a} \frac{h}{b} \kappa^{5/3} \frac{d}{d\kappa} \left(\kappa^{8/3} \gamma(\kappa) \right) .$$

Experimental measurements. Drag coefficient

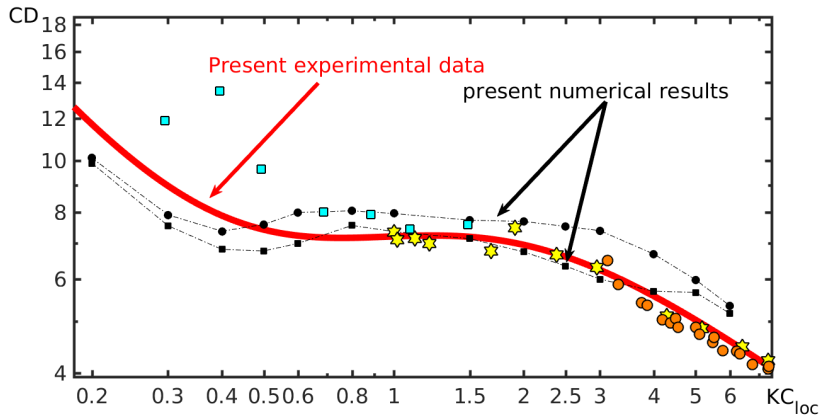


Figure : Drag coefficient C_D vs dimensionless amplitude KC_{loc} for chamfered edge beam

Publications

Numerical part of the research:

1. A.N. Nuriev, A.M. Kamalutdinov, A.G. Egorov. A numerical investigation of fluid flows induced by the oscillations of thin plates and evaluation of the associated hydrodynamic forces **Journal of Fluid Mechanics**, 2019 <https://doi.org/10.1017/jfm.2019.477>.
2. Nuriev A.N., Kamalutdinov A.M., Zaitseva O.N. Hydrodynamics around long vibrating beams. **Journal of Fluids and Structures**, 2020 Accepted with minor revision.

Experimental part of the research:

3. A.G. Egorov , A.M. Kamalutdinov, A.N. Nuriev Evaluation of aerodynamic forces acting on oscillating cantilever beams based on the study of the damped flexural vibration of aluminium test samples. **Journal of Sound and Vibration**, Volume 421, 2018, Pages 334–347 <https://doi.org/10.1016/j.jsv.2018.02.006>